Eleventh U.S. National Conference on Earthquake Engineering
Integrating Science, Engineering & Policy
June 25-29, 2018
Los Angeles, California

BUCKLING-INDUCED SHORTENING OF DEEP W-SHAPE COLUMNS IN SEISMIC STEEL FRAMES

G. Ozkula[1], J.L. Harris[2], and C.-M. Uang[3]

ABSTRACT

AISC Seismic Provisions specify a strong column-weak beam requirement for the design of special moment frames (SMF). But flexural hinging of columns at the base is permitted. Structural designers routinely specify deep, slender wide-flange columns (e.g., W24 or deeper sections) in SMF nowadays because their high moment of inertia about the strong-axis of bending is very efficient in reducing lateral story drifts to meet the code drift requirement. Deep column sections are characterized by a larger web slenderness (i.e., width-to-thickness) ratio than their stockier cross-section (e.g., W14) counterpart, which can result in significant local buckling in the plastic hinge. In addition, member slenderness is also higher, making a deep column vulnerable to out-of-plane buckling modes. A recent full-scale test program funded by the National Institute of Standards and Technology through a contract with the Applied Technology Council showed that deep columns that met the highly ductile compactness requirement specified in the AISC Seismic Provisions are prone to both local and lateral-torsional buckling under cyclic loading. Since typical software used by design engineers for performance-based seismic evaluation cannot simulate local buckling and the associated axial shortening, it is postulated that, as an alternative to bypass this limitation, dissipated energy computed at column ends by the software can be used to estimate the extent of buckling-induced axial shortening of deep columns. Based on results from both full-scale testing and numerical simulation, an expression is proposed that relates axial shortening to the column axial force, web width-thickness ratio, and normalized energy dissipation at the plastic hinge location.

[1] Postdoctoral Research Scientist, Dept. of Structural Engineering, Univ. of California, San Diego, La Jolla, CA, (gozkula@ucsd.edu)
[2] Research Structural Engineer, National Institute of Standards and Technology, U.S.A., (john.harris@nist.gov)
[3] Professor, Dept. of Structural Engineering, University of California, San Diego, La Jolla, CA, (cmu@ucsd.edu)

Buckling-Induced Shortening of Deep W-Shape Columns in Seismic Steel Frames

G. Ozkula[1], J.L. Harris[2], and C.-M. Uang[3]

ABSTRACT

AISC Seismic Provisions specify a strong column-weak beam requirement for the design of special moment frames (SMF). But flexural hinging of columns at the base is permitted. Structural designers routinely specify deep, slender wide-flange columns (e.g., W24 or deeper sections) in SMF nowadays because their high moment of inertia about the strong-axis of bending is very efficient in reducing lateral story drifts to meet the code drift requirement. Deep column sections are characterized by a larger web slenderness (i.e., width-to-thickness) ratio than their stockier cross-section (e.g., W14) counterpart, which can result in significant local buckling in the plastic hinge. In addition, member slenderness is also higher, making a deep column vulnerable to out-of-plane buckling modes. A recent full-scale test program funded by the National Institute of Standards and Technology through a contract with the Applied Technology Council showed that deep columns that met the highly ductile compactness requirement specified in the AISC Seismic Provisions are prone to both local and lateral-torsional buckling under cyclic loading. Since typical software used by design engineers for performance-based seismic evaluation cannot simulate local buckling and the associated axial shortening, it is postulated that, as an alternative to bypass this limitation, dissipated energy computed at column ends by the software can be used to estimate the extent of buckling-induced axial shortening of deep columns. Based on results from both full-scale testing and numerical simulation, an expression is proposed that relates axial shortening to the column axial force, web width-thickness ratio, and normalized energy dissipation at the plastic hinge location.

Introduction

Prior to the 1994 Northridge, California earthquake, it was common practice to use shallow wide-flange sections (e.g., W12 or W14) as columns in steel special moment frame (SMF) construction because of their small footprint; thereby maximizing architectural flexibility in floor layouts. Since the Northridge earthquake, engineers in the U.S. have turned to using deep, slender steel columns to achieve an economic design that satisfies code-enforced story drift requirements. However, since the slenderness ratios for local buckling and global buckling are significantly higher with deep columns, these columns are prone to various forms of buckling that impair their gravity load-carrying capacity [3, 4, 5]. Past research on the cyclic behavior of shallow (W14) columns (nominal depth =14 in.) under axial compression and cyclic drift for braced frame applications in high seismic regions was conducted by Newell and Uang [6]. Unfortunately, little research is available to support the seismic design or assessment provisions of deep columns in moment frame applications prescribed in AISC 341 [1] and ASCE 41 [7].

To fill this gap, NIST developed a comprehensive research plan to study the seismic behavior and design of deep, slender wide-flange steel beam-columns [8]. Experimental tests of

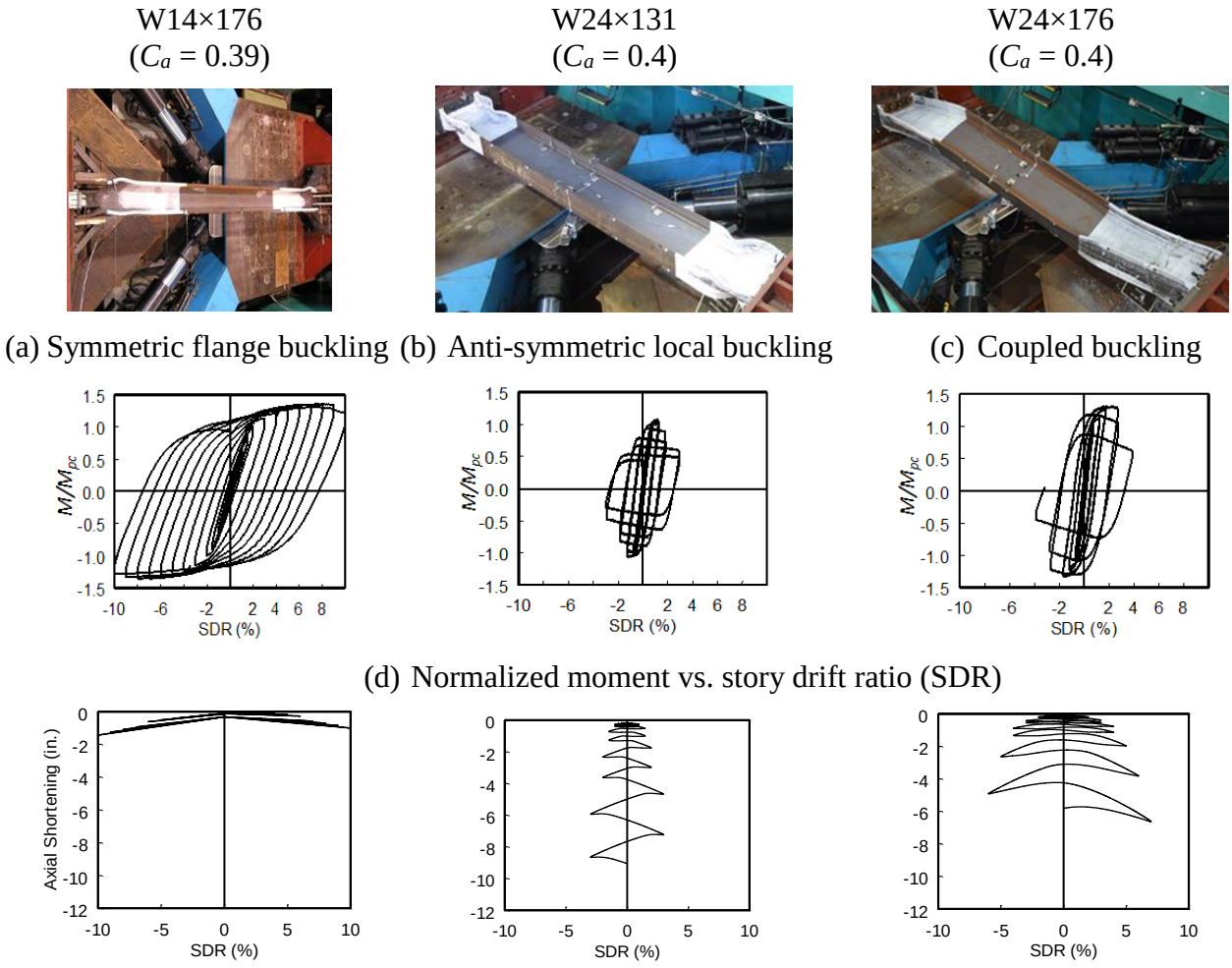

Figure 1 Column Cyclic Behavior and Axial Shortening of Different Failure Modes

deep columns were conducted at the University of California at San Diego (UCSD) [4, 9, 10]. ASTM A992 steel with a specified minimum yield stress of 50 ksi was used. Three levels of axial compression were considered: C_a = 0.2, 0.4, and 0.6, where C_a is the axial force ratio (= P / $\phi_c P_y$ with P = axial compression force, ϕ_c = 0.9, and P_y = nominal axial yield strength). Both constant and varying axial loads were considered in the test program to study the cyclic behavior of both interior and exterior columns in an SMF, respectively. A fixed-fixed end condition was used on most specimens, while some others were subjected to a fixed-flexible boundary condition, giving insights into the boundary condition effect.

Based on the test results from Newell and Uang [6] and NIST projects [5, 9, 10], it was observed that the cyclic response and axial shortening of a steel column is dependent on the governing buckling mode. The observed buckling behavior of all test specimens can be grouped into three categories–symmetric flange buckling (SFB), anti-symmetric local buckling (ALB), and coupled buckling (CB) [5]. These buckling modes are a function of the cross-sectional (local) and member (global) slenderness ratios of the column. Even under high axial load levels, a stocky W14 column could experience SFB and could reach a high story drift ratio (0.07 to 0.09 radians) with

minor strength degradation and local buckling. Limited or no web buckling would occur in this type of columns. Conversely, deep columns tend to experience ALB or CB, which is accompanied by significant strength degradation and buckling-induced axial shortening (see Figure 1).

Popov et al. [11] showed that considerable axial shortening may occur in a column with a compressive axial load before its lateral load-carrying capacity is lost. MacRea et al. [12, 13] studied axial shortening of columns under axial compression and cyclic lateral drifts. Experimental data from small-scale cantilever column tests were utilized to develop an empirical expression to estimate the amount of column axial shortening. Elkady and Lignos [14] evaluated the axial shortening of columns under combined axial loads and lateral cyclic drifts. It was observed that axial shortening increased substantially after local buckling occured.

Commercial continuum finite element analysis software (e.g., ABAQUS, LS-DYNA, and ANSYS) has the capability to perform nonlinear analysis of steel structures that captures large deflection behavior, local and global buckling, and axial shortening. For performance-based seismic evaluation, however, software with concentrated hinge component models or fiber-type models (e.g., PERFORM-3D, SAP 2000) are routine used by practicing engineers; this type of software cannot simulate axial shortening due to local or global buckling. As a first step to evaluating the effect of axial shortening on the safety margin against collapse of an SMF, an equation to predict axial shortening will be presented in this paper. Results from both cyclic tests and finite element simulations [15] were used to establish the proposed model.

Experimental Study

Full-scale column specimens were tested in a horizontal position with one end connected to a reaction fixture fixed to a strong wall. The other end of the column was connected to a reaction fixture on a shake table platen. The platen has six degrees of freedom. Longitudinal movement of the platen imposed an axial force to the test specimen. To evaluate the boundary condition effect, the platen also rotated in the plane for strong-axis bending of some column specimens. Cyclic loading protocol followed that specified in AISC 341 [1] for moment connection test. Figure 2 illustrates the range of flange and web slenderness ratios for all the specimens tested in the NIST and AISC projects, with dotted lines indicating seismic compactness limits specified in AISC 341. Table 1 shows the selected specimens that will be presented in this paper.

Typical Deep-Column Global Response versus Axial Shortening Relationship

Cyclic testing showed that deep columns would experience significant buckling and axial shortening even though the cross sections of these columns met the AISC 341 (2010b) highly ductile requirement for use in SMF. Significant shortening occurred because web local buckling interacted with flange local buckling. Figure 3(a) shows a typical axial shortening response, where the normalized axial shortening at one end of the column is presented. It was observed from both experimental tests and numerical simulation that axial shortening increased significantly when the normalized axial shortening reached 0.5%. In this study, the SDR corresponding to 0.5% normalized axial shortening is defined as the critical SDR. Figure 3(b) shows that this critical SDR usually corresponded to the peak strength of the column, beyond which a rapid strength degradation was accompanied by a rapid increase of axial shortening.

Figure 4 compares the axial shortening response of four specimens with increasing section slenderness ratios; the normalized axial compression remained the same (C_a = 0.2). All except Specimen 3L met the highly ductile requirement. As expected, the critical SDR tended to increase for more compact sections. But Specimens 2L and 3L experienced ALB and Specimens 15L and 1L experienced CB; the main cause of shortening is different.

Table 1 Test Matrix

Group No.	Shape	Specimen Designation [a]	Normalized Slenderness [b]			Column Axial Load	
			λ_f	λ_w	λ_L	C_a	P (kips)
1	W24×176	1L	0.67	0.57	1.42	0.2	465
		1M		0.61		0.4	931
		1H		0.66		0.6	1396
2	W24×131	2Z	0.93	0.66	1.46	0.0	0
		2L		0.70		0.2	347
		2L-P		0.70		0.2	347
		2M		0.76		0.4	693
		2H		0.82		0.6	1040
3	W24×104	3L	1.18	0.85	1.49	0.2	276
		3M		0.91		0.4	551
		3H		1.00		0.6	826
8	W24×131	8M	0.93	0.76	1.46	0.4	693
11	W24×176	11H-VA	4.81	28.7	71.05	0.6	Varies
		11H-BC					1396
13	W30×173	13M	7.04	40.8	63.16	0.4	916
		13M-BC					
15	W18×192	15L	3.27	16.7	77.42	0.2	506
16	W18×130	16M	4.65	23.9	80.0	0.4	690
		16M-BC					

[a] L for C_a = 0.2; M for C_a = 0.4; H for C_a = 0.6

[b] $\lambda_f = b_f/2t_f$, $\lambda_w = h/t_w$, $\lambda_L = L/r_y$

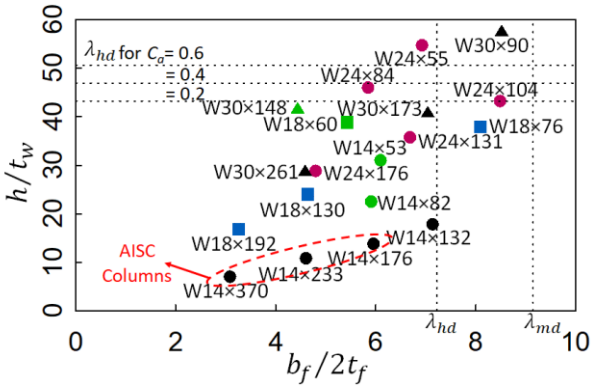

Figure 2 Width-to-thickness ratios of Test Specimens

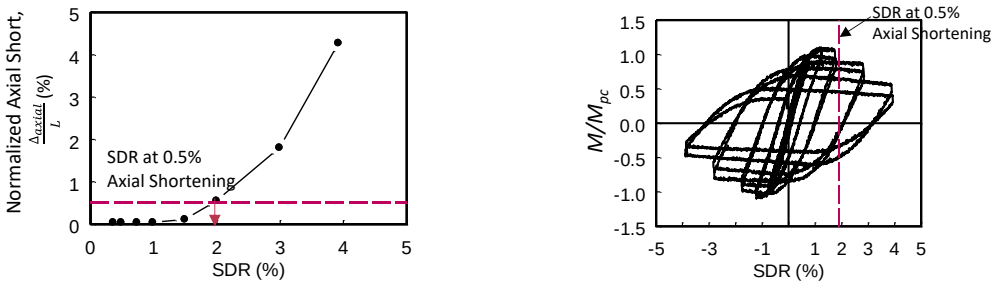

(a) Axial Shortening vs. SDR (b) Moment-Rotation Curve

Figure 3 Typical Global Response versus Axial Shortening Relationship (Specimen 4L)

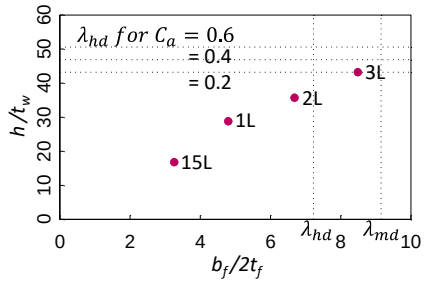

(a) Width-to-thickness ratios

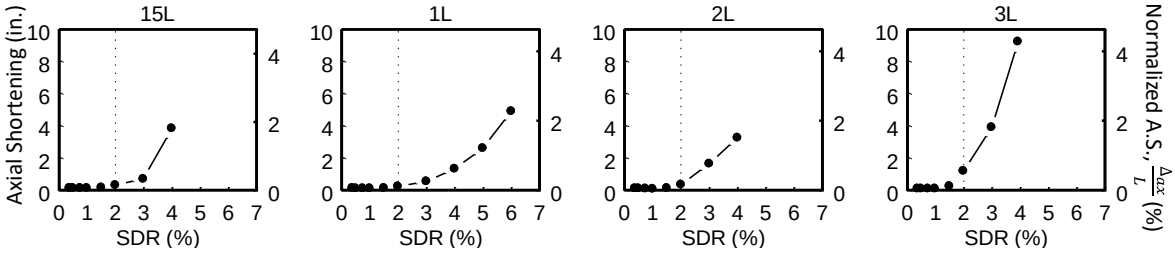

(b) Axial Shortening versus SDR

Figure 4 Normalized Axial Shortening and Slenderness Ratios

Axial Force Effect

Level of Axial Force

Two plots are presented for Group 2 specimens in Figure 5. These three specimens were each subjected to a constant axial compression, but the force level was different. The first plot compares shortenings measured at the end of each test, while the second plot compares shortenings observed at the same drift level to show the effect of axial force. It is evident from Figure 5(b) that the amount of axial shortening is very sensitive to the level of axial load.

Varying Axial Force

Figure 6(a) shows the backbone curve comparison between Specimen 1H subjected to a constant axial compression (C_a = 0.6), representative of an interior column, and Specimen 11H-VA subjected to a varying axial load, representative of an exterior column. The maximum strength increased in the varying axial load case. In addition, since the demand was smaller for the column subjected to a varying axial load, local buckling initiation was delayed. Figure 6(c) illustrates that axial shortening of Specimen 1H is three times that of Specimen 11H-VA. This comparison

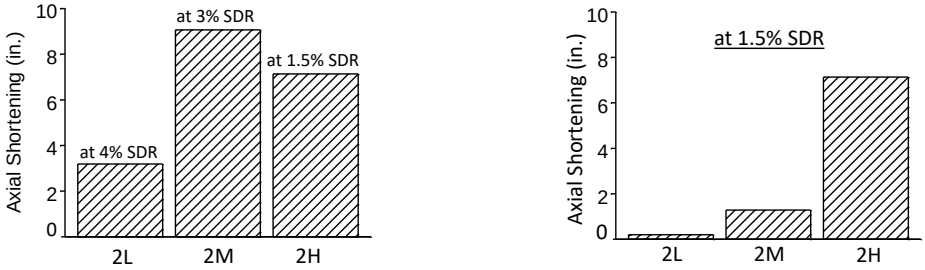

(a) at End of Test (b) at 1.5% SDR

Figure 5 Column Axial Shortening (Group 2 Specimens)

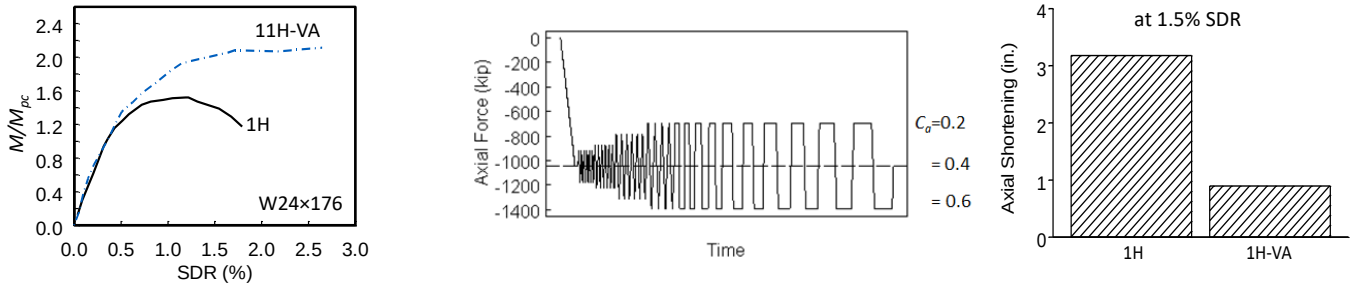

(a) Normalized Moment vs. SDR (%) (b) Axial Load Variation (c) Axial Shortening

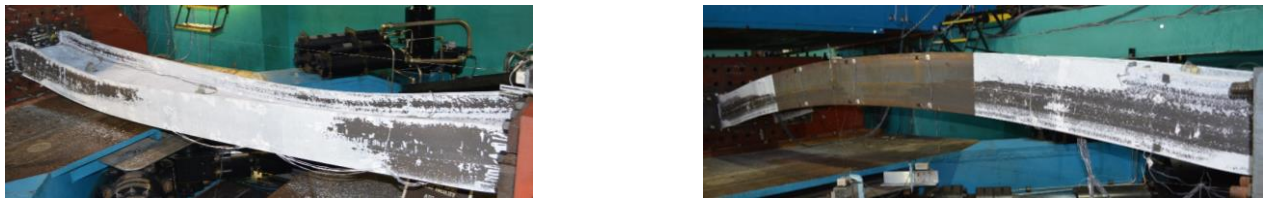

(a) Specimen 11H-VA (b) Specimen 1H

Figure 6 Varying Axial Force vs. Constant Axial Force

indicates that the cyclic behavior of these columns is very different in terms of maximum strength, post-buckling flexural strengths, strength deterioration rate, and axial shortening. Different axial shortenings between interior and exterior columns can also increase the flexural demand on the supported beams.

Loading Protocol Effects

Monotonic vs. Cyclic Loading

Figure 7 illustrates the effect of cyclic loading by comparing the cyclic response of two nominally identical specimens (2L and 2L-P). Both specimens experienced ALB. At 4% SDR, the monotonically loaded specimen 2L-P showed minor local buckling at one flange, and the axial shortening was 0.5 in. On the other hand, the cyclically loaded Specimen 2L had a 3.2-in. axial shortening at 4% SDR. The effect of cyclic loading is very significant.

Once Specimen 2L-P was loaded monotonically to 4% drift, testing continued with a reversed AISC loading protocol, i.e., the drift decreased in amplitude; the response is designated as "2L-P (Reversed AISC)" in the figure. Figure 7(b) shows that Specimen 2L-P exhibited an axial shortening 43% larger than that of Specimen 2L, indicating that axial shortening is also affected by the sequence of cyclic loading.

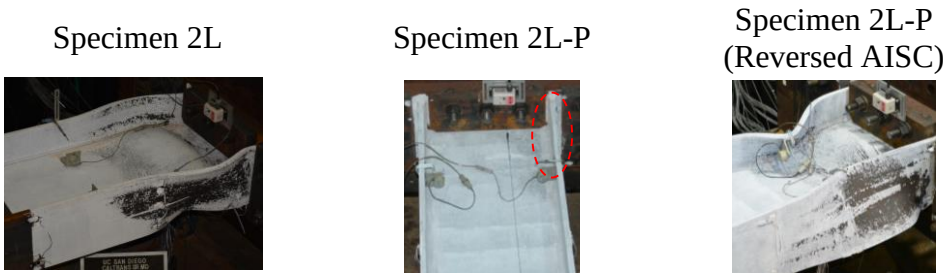

(a) Local Buckling Pattern

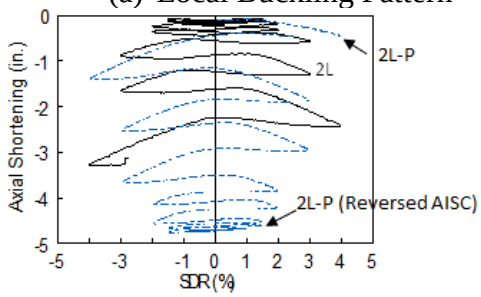

(b) Axial Shortening

Figure 7 Monotonic vs. Cyclic Loading Effect (W24×131 Specimens)

Far-field versus Near-fault Loading

Comparison can be made between the performance of two nominally identical specimens (2M and 8M) to evaluate the far-field versus near-fault loading effect. Figure 8(a) depicts the global behavior comparison between the symmetric far-field loading protocol and near-fault loading protocol. Local buckling, and consequently axial shortening, was more severe for the far-field loading case, although the amount of energy dissipation was similar. Figure 8(c) shows that the large pulses in the early stage of near-fault loading contributed to about one-third of the total shortening; the trailing cycles after the largest pulse also contributed significantly to the shortening.

Boundary Condition Effects

Two pairs of specimens (Groups 13 and 16) were used to evaluate the boundary condition effect. For each pair, one of the two nominally identical specimens was tested in a fixed-fixed boundary condition, while the other (designed with "BC") was tested with one end fixed and the other end allowed to rotate with an angle equal in magnitude to the SDR. Axial shortening presented in Figure 9 represents that measured axial shortening for the entire column. Because the fixed-fixed case showed two plastic hinges while the fixed-flexible case had only one plastic hinge, column axial shortening of the former case was about twice that of the latter case. Therefore, test results from the fixed-fixed case can be used to predict axial shortening of one plastic hinge, and the results can be applied to cases when only one plastic hinge is formed at the bottom end of the first-story column.

Determination of Axial Shortening

Experimental results showed that axial shortening is affected by the magnitude and number of cycles, indicating that cumulative ductility needs to be considered. In this study, cumulative ductility is measured by the normalized energy, η, defined as Eq. 1.

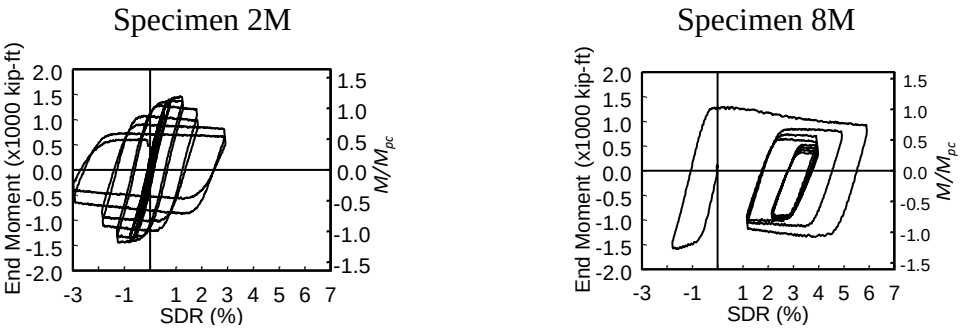

(a) Hysteresis Response

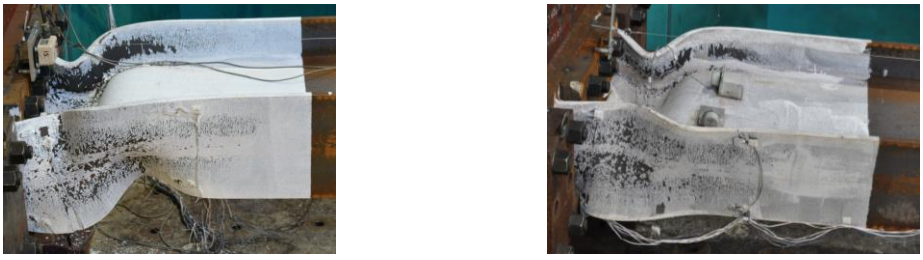

(b) Local Buckling Pattern

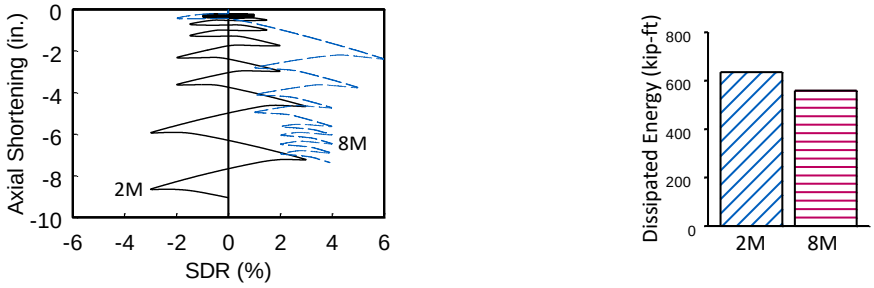

(c) Axial Shortening (d) Energy Dissipation

Figure 8 Comparison of Response between Far-field and Near-fault Ground Motions

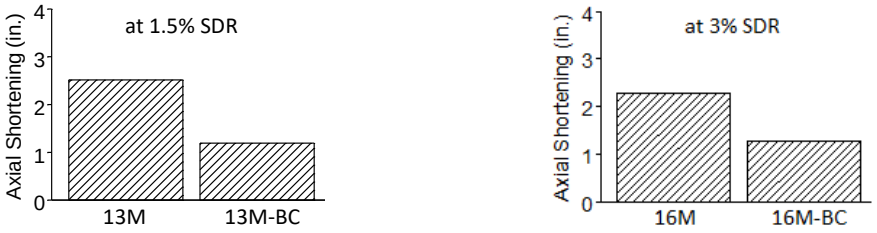

(a) Group 13 (W30×173) (b) Group 16 (W18×130)

Figure 9 Boundary Condition Effect on Axial Shortening

$$\eta = \frac{E_h}{M_p} \tag{1}$$

where M_p is the plastic moment capacity of the section, and E_h is the cumulative hysteretic energy given by Eq. (2).

$$E_h = \int M_{end} d\theta \tag{2}$$

For the fixed-fixed case, M_{end} is the moment at the column end, and θ is the SDR in radians. The

normalized axial shortening Δ_{axial} / L, where L is the column length of one plastic hinge is plotted against the normalized energy, η, for two sample column specimens in Figure 10. The axial shortening at η = 0 corresponds to the elastic axial shortening due to the applied axial compression. The relationship between the normalized axial shortening and η can be expressed by the exponential form given in Eq. (3).

$$\frac{\Delta_{axial}}{L} = \alpha e^{\beta\eta} \tag{3}$$

where α is the elastic axial strain due to the constant axial compression given by Eq. 4.

$$\alpha = \frac{P}{EA} \tag{4}$$

Parameter β for each specimen can be determined by curve fitting to measured data. A total of 19 data points from cyclic testing in this NIST project were evaluated. To enhance the database, an additional 96 numerically simulated cases were also considered [15]. Since the β value is a function of many parameters, including the magnitude of axial force as well as the section and member slenderness ratios, a stepwise multivariate regression analysis was performed to identify the most influential parameters. The regression analysis resulted in the expression for β given in Eq. (5).

$$\beta = C\left(\frac{h}{t_w}\right)^{1.56}\left(1 - \frac{P_u}{P_y}\right)^{-2.1} \tag{5}$$

where C is taken as 0.028 and 0.022 for ALB and CB, respectively; see [5] for a proposed procedure to classify the governing buckling mode. The coefficient of determination is R^2=93%.

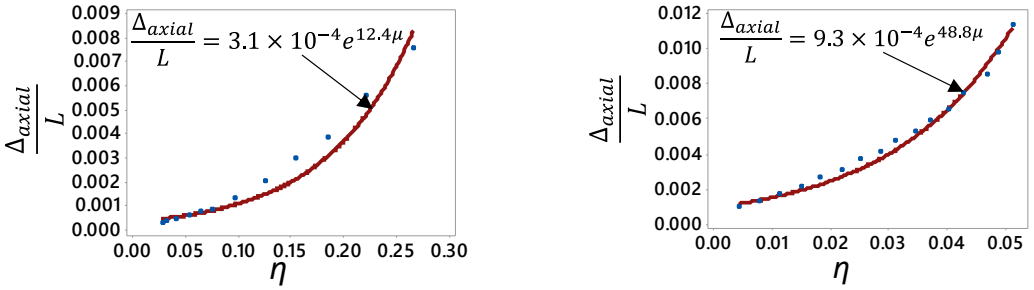

(a) Specimen 2L (b) Specimen 3H

Figure 10 Normalized Axial Shortening versus Normalized Cumulative Energy

(a) Test Results (b) Simulation Results

Figure 11 Comparison of Predicted versus Measured Normalized Axial Shortening

To demonstrate the accuracy of Eq. 3. Figure 11 (a) shows a comparison to the axial shortening of the 19 test specimens at different drift levels while Figure 11(b) shows a similar comparison for the 96 simulated columns.

Conclusions

While deep wide-flange columns are favored by design engineers nowadays to meet the code story drift requirement for special moment frame design, recent testing showed that deep columns that meet the AISC highly ductile requirement are prone to local buckling and out-of-plane lateral-torsional buckling, which in turn resulted in significant axial shortening. Test data showed that axial shortening can be expressed as a function of the constant axial compression force, web width-thickness ratio, and normalized dissipated energy (Eq. 3). Though interaction between flange and web buckling was observed, flange slenderness is not directly required since there exists a correlation between the two slenderness parameters. To determine the coefficients in this equation by regression analysis, the test database was augmented by high-fidelity finite element simulation of 96 columns. Since typical software used by designers for performance-based seismic evaluation cannot simulate local buckling and axial shortening, it is postulated that, as an alternative to bypass this limitation, dissipated energy computed at the column ends by the software can be used to estimate buckling-induced axial shortening of deep columns. The proposed equation applies to columns with constant axial load only, which is typical of interior columns in a moment frame. A similar equation applicable for exterior columns with varying axial load demands remains to be developed.

Acknowledgement

Funding for this research was provided by the ATC under a contract with the NIST. Jim Malley from Degenkolb Engineers chaired the Project Advisory Committee. A. Hortacsu from ATC served as the Project Manager. The authors would like to acknowledge AISC for providing steel materials and The Herrick Corporation for providing fabrication of the test specimens. The W14 column test program was sponsored by AISC.

Disclaimer

NIST policy is to use the International System of Units (metric units) in all its publications. In this paper, however, information is presented in U.S. Customary Units (inch-pound), as this is the preferred system of units in the U.S. earthquake engineering industry.

Certain commercial software, equipment, instruments, or materials may have been used in the preparation of information contributing to this paper. Identification in this paper is not intended to imply recommendation or endorsement by NIST, nor is it intended to imply that such software, equipment, instruments, or materials are necessarily the best available for the purpose.

No formal investigation to evaluate potential sources of uncertainty or error, or whether multiple sources of error are correlated, was included in this study. The question of uncertainties in the analytical models, solution algorithms, material properties and as-built dimensions and positions of members versus design configurations employed in analysis are beyond the scope of the work reported here.

References

1. AISC. (2016). *Seismic provisions for structural steel buildings,* ANSI/AISC 341-16, American Institute of Steel Construction Chicago, IL.
2. AISC. (2016). *Prequalified Connections for Special and Intermediate Steel Moment Frames for Seismic Applications,* ANSI/AISC 358-16, American Institute of Steel Construction, Chicago, IL.

3. Fogarty, J., and El-Tawil, S. (2016). "Collapse resistance of steel columns under combined axial and lateral loading." *Journal of Structural Engineering*, Vol. 142, No. 1, ASCE.
4. Ozkula, G., Harris, J., and Uang, C.-M. (2017). "Observations from cyclic tests on deep, wide-flange beam-columns." *Engineering Journal*, 1st Quarter, AISC, 45-59.
5. Ozkula, G., Harris, J., and Uang, C.-M. (2017). "Classifying cyclic buckling modes of steel wide-flange columns under cyclic loading." *Structures Congress*, 155-167, ASCE/SEI, Reston, VA.
6. Newell, J.D., and Uang, C.-M. (2008). "Cyclic behavior of steel wide-flange columns subjected to large drift," *Journal of Structural Engineering*, Vol. 134, No. 8, 1334-1342, ASCE.
7. ASCE. (2013). *Seismic rehabilitation of existing buildings*, ASCE 41, American Society of Civil Engineers, Reston, VA.
8. NEHRP. (2011). "Research plan for the study of seismic behavior and design of deep, slender, wide flange structural steel beam-column members" *NIST-GCR-11-917-13*, Gaithersburg, MD.
9. Ozkula, G., and Uang, C.-M. (2015). "ATC 106 Phase I: Seismic behavior and design of deep, slender wide-flange structural steel beam-column members." *Rep. No. SSRP-15/06*, Department of Structural Engineering, University of California, San Diego, La Jolla, CA.
10. Ozkula, G., Chansuk, P., and Uang, C.-M. (2017). "ATC 106 Phase II: Seismic behavior and design of deep, slender wide-flange structural steel beam-column members." *Rep. No. SSRP-17/04*, Department of Structural Engineering, University of California, San Diego, La Jolla, CA.
11. Popov, E.P., Bertero, V.V., and Chandramouli, S. (1975). "Hysteretic behavior of steel columns." *Report No. UCB/EEC*, Earthquake Engineering Research Center, University of California.
12. MacRae, G. (1990). "The seismic response of steel frames." *Report No. 90-6*, Department of Civil Engineering, University of Canterbury, New Zealand.
13. MacRae, G., Urmson, C.R., Walpole, W.R., Moss, P., Hyde, K., and Cliftoon C. (2009). "Axial shortening of steel columns in buildings subjected to earthquakes." *Bulletin of the New Zealand Society for Earthquake Engineering*, Vol. 42, No. 4.
14. Elkady, A., and Lignos, D. G. (2015). "Analytical investigation of the cyclic behavior and plastic hinge formation in deep wide-flange steel beam-columns." *Bulletin of Earthquake Engineering*, 13(4), 1097-1118.
15. Ozkula, G. (2017). Seismic behavior, modeling, and design of deep wide-flange steel columns for special moment frames, *Ph.D thesis*, University of California, San Diego, La Jolla, CA.